Polyrhythmic synchronization in bursting networking motifs

Andrey Shilnikov,[a] René Gordon, and Igor Belykh
Department of Mathematics and Statistics and The Neuroscience Institute, Georgia State University, 30 Pryor Street, Atlanta, Georgia 30303, USA

(Received 3 March 2008; accepted 25 June 2008; published online 22 September 2008)

We study the emergence of polyrhythmic dynamics of motifs which are the building block for small inhibitory-excitatory networks, such as central pattern generators controlling various locomotive behaviors of animals. We discover that the pacemaker determining the specific rhythm of such a network composed of realistic Hodgkin–Huxley-type neurons is identified through the order parameter, which is the ratio of the neurons' burst durations or of duty cycles. We analyze different configurations of the motifs and describe the universal mechanisms for synergetics of the bursting patterns. We discuss also the multistability of inhibitory networks that results in polyrhythmicity of its emergent synchronous behaviors. © *2008 American Institute of Physics*.
[DOI: 10.1063/1.2959850]

The emergence of synchronous rhythms in the networks in question is closely tied to the temporal characteristics of the bursting neurons due to their intrinsic properties, or to synaptic coupling types as inhibitory and excitatory. When the individual neuron is close to the transition from bursting into tonic spiking, the dynamics of the network become quite sensitive to small changes in synaptic coupling strengths. We reveal the way the network can alter the burst durations of its neurons to designate the pacemakers among them. This endows the network with flexible synchronization properties leading to the multistability of coexistent bursting rhythms. In this paper, we describe a universal burst-duration based mechanism of the emergence of various synchronous bursting patterns in the basic repetitive blocks (motifs) for larger realistic neuronal networks such as central pattern generators (CPGs) controlling locomotion activities in animals and humans.

I. INTRODUCTION

A large variety of biological functions are accomplished through highly coordinated actions of interneurons. Thus, the origin of many biological rhythms can be attributed to synchronous rhythmic outputs from networks of coupled excitable interneurons and/or neurons. For example, heartbeats result from orchestrated activities of muscle interneurons,[1] hormonal rhythms are driven by rhythmic outputs from networks of endocrine neurons in the hypothalamus, and patterns of lamprey locomotion are produced by a central pattern generator (CPG) located in the spinal cord of the animal.[2] The presence of synchronization has also been shown in special areas such as the olfactory system or the hippocampal region.[3–5]

Bursting occurs when neuron activity alternates, on a slow time scale, between a quiescent state and fast repetitive spiking. Different types of bursting and mechanisms of their generation have been extensively studied.[6–12] When coupled, bursting neurons may exhibit different forms of synchrony, including synchronization of individual spikes, burst synchronization when only the envelopes of the spikes synchronize, and complete synchrony.[13–16]

Neural synchronization results from the interplay between the intrinsic properties of the individual neurons, the properties of the synaptic coupling, as well as the network topology.[13–26] Each property may play an important role in shaping the emergent synchronous behavior. Different bursters, for example, have different synchronization properties. While elliptic bursters are relatively easy to synchronize, square-wave and parabolic bursters are notorious for their resistance to synchronization.[13] Inhibitory and excitatory synapses also play different roles in promoting synchronization or antisynchronization of bursting neurons.[17–23] It has been shown that the synchronizing roles of inhibition and excitation depend on the rates of onset and decay of inhibition with respect to the intrinsic timescale of the individual neurons. More precisely, fast excitation often produces synchrony, whereas fast direct inhibition typically desynchronizes neurons.[27]

The underlying coupling structure of a neural network also affects its synchronization properties. Fast inhibition, for example, triggers antisynchronous behavior in a pair of reciprocally coupled bursters.[17] On the other hand, common fast inhibition of a neuronal network received from a pacemaker neuron may induce synchronization in the network.[24,28] CPGs of motor interneuronal networks are often composed of pairs of reciprocally inhibiting neurons, driven by a common bursting inhibitor.[29] Therefore, the "competition" between the desynchronizing and synchronizing factors leads to the emergence of different synchronous and asynchronous rhythms in such networks. An important problem is to determine the precise role each factor plays in generating the synchronous rhythms. This problem becomes more challenging when the neural network has a complex topology and is composed of both inhibitory and excitatory

[a]Author to whom correspondence should be addressed. Electronic mail: ashilnikov@gsu.edu.

neurons. It was hypothesized that complex and highly evolved neural networks arise from the addition of network elements in positions where they maximize the overall processing power of the network topology.[30] To gain insight into the rules governing pattern formation in complex networks of neurons, one should first investigate the rules underlying the emergence of cooperative rhythms in smaller network building blocks. These building blocks called *motifs* are typically three-node networks. Their functional and structural importance has been examined in biological networks of a different nature. For example, in information processing networks motifs are believed to have specific functions as elementary computational circuits.[31]

Synchronization in complex oscillator networks and their structural motifs has received a great deal of attention in mathematical and physical literature.[32–36] One important cooperative rhythm is clustering[37–40] (also known as polysynchronization[41]) when the network of oscillators splits into subgroups, called clusters, such that all oscillators within one cluster move in perfect synchrony. The existence of the clusters is due to the intrinsic symmetries of the idealized mathematical models.[39–41]

Due to multiple time scales of the endogenous bursting neurons, bursting networks may exhibit richer cooperative dynamics. This includes the emergence of clusters of burst synchronized rhythms. For realistic neural CPG, which is formed by nonidentical interneurons with different burst durations and with strongly heterogeneous connections, one has to redefine burst synchronization as the process where interneurons start bursting nearly instantly, though cease bursting individually at different times. The appearance of such coordinated bursting rhythms is not defined by the symmetries but rather by the dynamical properties of the individual neurons and synaptic couplings. We call it *polyrhythmic* synchronization.

The aim of this paper is to investigate the conditions under which specific patterns of polyrhythmicity appear in network motifs that are the characteristic building blocks composing CPGs and other neural circuits. While studying simple inhibitory networks, we discovered recently[28] that the ratio of the neurons' burst durations is the critical characteristic, explicitly defining synchronization properties of the network. In particular, we demonstrated that a bursting network with strongly desynchronizing connections can be synchronized by a weak common inhibitory input from an external pacemaker neuron whose burst duration is sufficiently long.[28] Therefore, the ratio of the burst durations becomes the imperative order parameter that controls the cooperative dynamics of the network and designates its pacemaker by the intrinsic properties of the individual neurons.

In this paper, we go further and target interneuron networks with both inhibitory and excitatory synapses. We study polyrhythmic synchronization in different bursting motifs and show, in particular, that when the state of the individual neuron is close to the transition from bursting into tonic spiking, excitatory coupling can essentially increase the burst duration of the given neuron, whereas the inhibition shortens the burst durations of the other interneurons in the motif. The longest neuron is thus designated as a pacemaker that induces a synchronous rhythm over the network. This effect of the emergent network behavior shows how single neurons initially having shorter burst durations can self-organize to create a pacemaker with a longer burst duration that, in turn, induces synchronous rhythms in the network.

The layout of this paper is as follows: In Sec. II, we introduce the model and describe its phase space and bifurcation diagram. We describe, in particular, how applied external excitation or inhibition can affect the dynamics of the system. In Secs. III and IV, we study cooperative behavior of network motifs and describe the principles that are critical for controlling synchronous rhythms in the network. These include the "lock-down-then-release" mechanism of the alternation of bursting's onset in a pair of reciprocally inhibiting interneurons[22,42] and the ability of excitatory (inhibitory) coupling to increase (decrease) the burst duration of the driven neuron. Section III focuses on two- and three-interneuron inhibitory motifs, while Sec. IV discusses multistability and control of polyrhythmicity in inhibitory-excitatory motifs and larger networks. Section V discusses the obtained results and further directions.

II. NETWORKED INTERNEURON MODEL

We study inhibitory-excitatory networks composed of several reduced models of the leech heart interneuron,[10–12,43] whose derivation follows the Hodgkin–Huxley formalism

$$C\frac{dV_i}{dt} = -[I_{\mathrm{Na}} + I_{\mathrm{K2}} + I_{\mathrm{leak}} + I_{\mathrm{pol}} + I_{\mathrm{syn}}],$$

$$\tau_{\mathrm{Na}}\frac{dh_i}{dt} = f(500, 0.033\,91, V_i) - h_i, \tag{1}$$

$$\tau_{\mathrm{K2}}\frac{dm_i}{dt} = f(-83, 0.018 + V_{\mathrm{K2}}^{\mathrm{shift}}, V_i) - m_i,$$

with

$$\begin{aligned} I_{\mathrm{Na}} &= \bar{g}_{\mathrm{Na}} f(-150, 0.0305, V_i)^3 h_i (V_i - E_{\mathrm{Na}}), \\ I_{\mathrm{K2}} &= \bar{g}_{\mathrm{K2}} m_i^2 (V_i - E_{\mathrm{K}}), \\ I_{\mathrm{leak}} &= g_{\mathrm{leak}} (V_i - E_{\mathrm{leak}}), \\ I_{\mathrm{syn}} &= I_{\mathrm{syn}}^{\mathrm{inh}} + I_{\mathrm{syn}}^{\mathrm{exc}} \\ &= -\sum_{j=1}^{n} [g_{ij}^{\mathrm{in}} (E_{\mathrm{syn}}^{\mathrm{inh}} - V_i) + g_{ij}^{\mathrm{exc}} (E_{\mathrm{syn}}^{\mathrm{exc}} - V_i)] \Gamma(V_j - \Theta_{\mathrm{syn}}), \end{aligned} \tag{2}$$

where V_i is the membrane potential, m_i and h_i are the gating variables describing the activation of the potassium I_{K2} and inactivation of the sodium current I_{Na} of the ith interneuron, respectively. Other parameters: $C=0.5$ nF is the membrane capacitance; $\bar{g}_{\mathrm{K2}}=30$ nS is the maximum conductance of I_{K2}; $E_{\mathrm{K}}=-0.07$ V and $E_{\mathrm{Na}}=0.045$ V are the reversal potentials of K^+ and Na^+, respectively; $\bar{g}_{\mathrm{Na}}=200$ nS is the maximal conductance of I_{Na}; $g_l=8$ nS and $E_{\mathrm{leak}}=-0.046$ V are the conductance and reversal potential of the leak current; the polarization current is constant $I_{\mathrm{pol}}=0.001$ mA; and the time constants are $\tau_{\mathrm{K2}}=0.9$ s $\tau_{\mathrm{Na}}=0.0405$ s; $f(x,y,z)$

$=1/(1+\exp\{x(y+z)\}$ is a Boltzmann function describing kinetics of the currents.

The reversal potential $E_{\rm syn}^{\rm inh}=-0.0625$ ($E_{\rm syn}^{\rm exc}=0.04$) is set to be smaller (larger) than $V_i(t)$ along each bounded solution, i.e., the synapse is assumed to be inhibitory (excitatory). Note that connectivity matrices defined by $g_{ij}^{\rm in}$ and $g_{ij}^{\rm exc}$ are independent such that each pair of interneurons i and j may have both inhibitory and excitatory connections. The synaptic coupling function is modeled by the sigmoidal function $\Gamma(V_j)=1/\{1+\exp[-1000(V_j-\Theta_{\rm syn})]\}$.[44] It is worth noticing here that we have tested not only this sufficient algebraic representation but also high-order differential equations to model each fast synaptic current and found no principal distinction in cooperative dynamics for our purposes. The threshold $\Theta_{\rm syn}=-0.03$ is chosen so that every spike within a burst of the neuron burst can reach it. This implies that the synaptic current from the jth neuron is initiated as soon as this neuron becomes active after its membrane potential exceeds the synaptic threshold.

In network (1), the neurons are identical and the synapses are fast and instantaneous.[16] For simplicity, the heterogeneity is introduced to the system via the synapses; coupling coefficients $g_{ij}^{\rm in}$ and $g_{ij}^{\rm exc}$ are, in general, different for each interneuron. So, when coupled, the neurons typically receive different amounts of excitation and inhibition and therefore exhibit nonidentical dynamics.

Due to the disparity of the time constants of the currents in the model, it can be treated as a fast-slow system; its first two differential equations, describing the voltage and the sodium kinetics, form a fast subsystem, while the last equation, describing the evolution of the potassium current, is the slow one. The dynamics of a slow-fast system are known[45–47] to be centered around the attracting pieces of the slow motion manifolds, which determine skeletons of activity patterns. These manifolds, which are composed of equilibria and limit cycles of the fast subsystem, can also be found as the corresponding $V_{\rm K2}^{\rm shift}$-parametric branches on the full system. A typical *bursting* Hodgkin–Huxley model should correspondingly possess a pair of such manifolds:[6] a Z-shaped quiescent manifold and a cylinder-shaped tonic spiking one (Fig. 1). Whenever the spiking $M_{\rm lc}$ and quiescent $M_{\rm lc}$ manifold are transient for the solutions of Eq. (1), the model exhibits bursting, represented by a solution repeatedly switching between the low, hyperpolarized branch of $M_{\rm eq}$ and the spiking manifold $M_{\rm lc}$. The hyperpolarized fold on $M_{\rm eq}$ indicates the beginning of a burst. A similar fold on $M_{\rm lc}$ indicated the termination of the spiking phase of the burst. The number of complete revolutions of the solution between the folds is that of spikes per burst. This winding number is used to classify the bursting activity. The larger the number, the longer the burst duration lasts.

A. Phase space and bifurcation diagram

The interneuron's intrinsic bifurcation parameter $V_{\rm K2}^{\rm shift}$ is a deviation from the mean, experimentally identified voltage $V_{1/2}=0.018$ V corresponding to the semiactivated potassium channel, i.e., $f_\infty=1/2$ for $I_{\rm K2}$. In this study, the range of $V_{\rm K2}^{\rm shift}$ is $[-0.03;0.005]$ V. One sees from the slow equation of Eq.

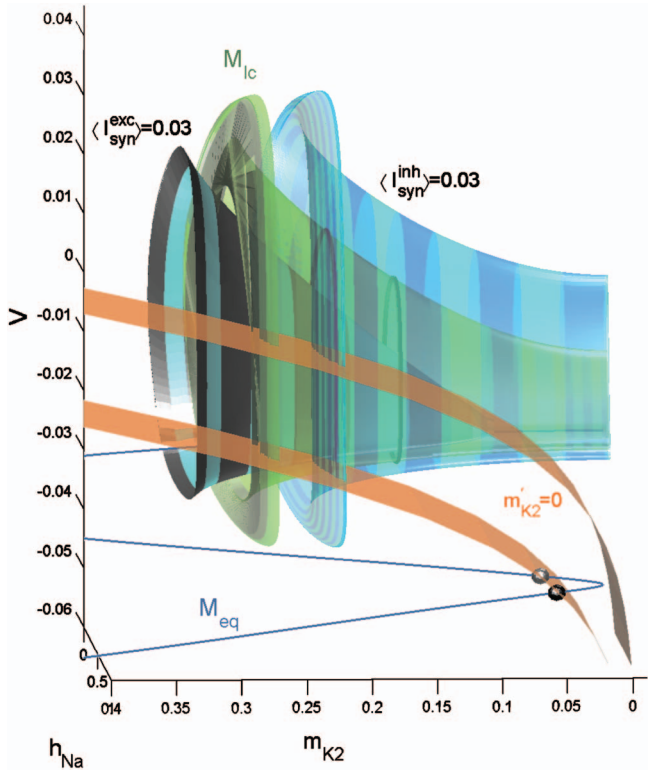

FIG. 1. (Color) Spiking $M_{\rm lc}$ and quiescent $M_{\rm eq}$ slow motion manifolds along with the slow nullcline $m'=0$ in the phase space of model (1) for $V_{\rm K2}^{\rm shift}=-0.005$ V (lower brown surface) and -0.024 V (upper). The spiking manifold $M_{\rm lc}$ is shown for three effective synaptic currents $\langle I_{\rm syn}^{\rm exc}\rangle=0.03, \langle I_{\rm syn}\rangle=0, \langle I_{\rm syn}^{\rm inh}\rangle=0.03$, respectively. Increasing $V_{\rm K2}^{\rm shift}$, or raising the inhibitory synaptic current $\langle I_{\rm syn}^{\rm inh}\rangle$ hyperpolarizes the interneuron. The new stable equilibrium state at the intersection of the nullcline $m'=0$ with the low, hyperpolarized branch of $M_{\rm eq}$ corresponds to the locked-down state of the interneuron. In contrast, decreasing $V_{\rm K2}^{\rm shift}$, or raising $\langle I_{\rm syn}^{\rm exc}\rangle$ brings both nullclines $m'=0$ and $M_{\rm lc}$ closer, thus slowing down the potassium current. This may further result in the emergence of a stable periodic orbit around $M_{\rm lc}$ corresponding to the tonic spiking activity of the interneuron.

(1) that variations of $V_{\rm K2}^{\rm shift}$ translate the slow nullcline $m'=0$ in the V-direction. Let us note that the burst duration $\tau_{\rm bd}$, or the interburst interval $\tau_{\rm ii}$, is longer the smaller the distance between the slow nullcline $m'=0$ and the corresponding tonic spiking $M_{\rm lc}$ or quiescent $M_{\rm eq}$ manifolds is, and vice versa. Decreasing $V_{\rm K2}^{\rm shift}$ elevates the slow nullcline $m'=0$ thereby slowing down further the slow translation of the m-component of the phase point coiling around $M_{\rm lc}$. Further decreasing $V_{\rm K2}^{\rm shift}$ will eventually stop the activation of $I_{\rm K2}$ making the tonic spiking manifold $M_{\rm lc}$ nontransient for solutions of Eq. (1). This occurs after a saddle-node bifurcation for periodic orbits, leading to the emergence of two periodic orbits on $M_{\rm lc}$; the stable one corresponds to the tonic spiking activity of the interneuron. So, the interneuron fires tonically at the lower $V_{\rm K2}^{\rm shift}$ values, while its larger values correspond to the hyperpolarized quiescent state, see Figs. 1 and 2. Observe first that the equilibrium state of the individual neuron model is that of its fast subsystem. In the phase space of Eq. (1) it is an intersection point of the 1D quiescent manifold $M_{\rm eq}$ with the 2D slow nullcline $m'=0$, see Fig. 1. By construction, the intersection point on the bottom branch of $M_{\rm eq}$ is the stable equilibrium state, represented by the blue sphere in Fig. 1 and corresponding to the locked-down hyperpolar-

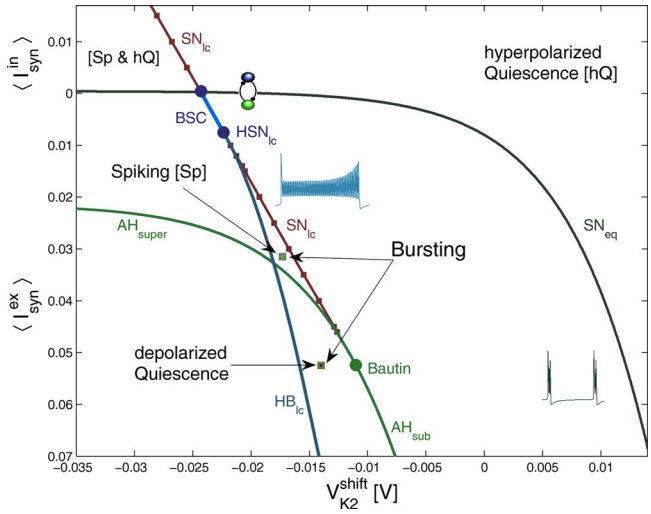

FIG. 2. (Color online) $(V_{K2}^{shift}, \langle I_{syn}\rangle)$ bifurcation plane partitioned into the zones of activity of the interneuron model (1). Above the boundary SN_{eq} the interneuron is locked down at the hyperpolarized state by influx of the inhibitory synaptic current. Bursting takes place between the bifurcation curves $BSC \cup HB_{lc}$ and SN_{eq}. To the left of SN_{lc}, corresponding to the saddle-node bifurcation of the periodic orbits, the interneuron gets into tonic spiking. The spiking zone is also bounded by the boundary labeled AH, below which the neuron is constantly depolarized. The *Bautin* point is where the corresponding Andronov–Hopf bifurcation changes from the super- to subcritical type. In the wedge within SN_{lc} and HB_{lc}, bursting co-exists with tonic spiking (above AH_{super}) or depolarized quiescence (below it). The model becomes monoactive to the left of HB_{lc}, where the stable manifold of the saddle periodic orbit no longer separates the basins of the attractors.

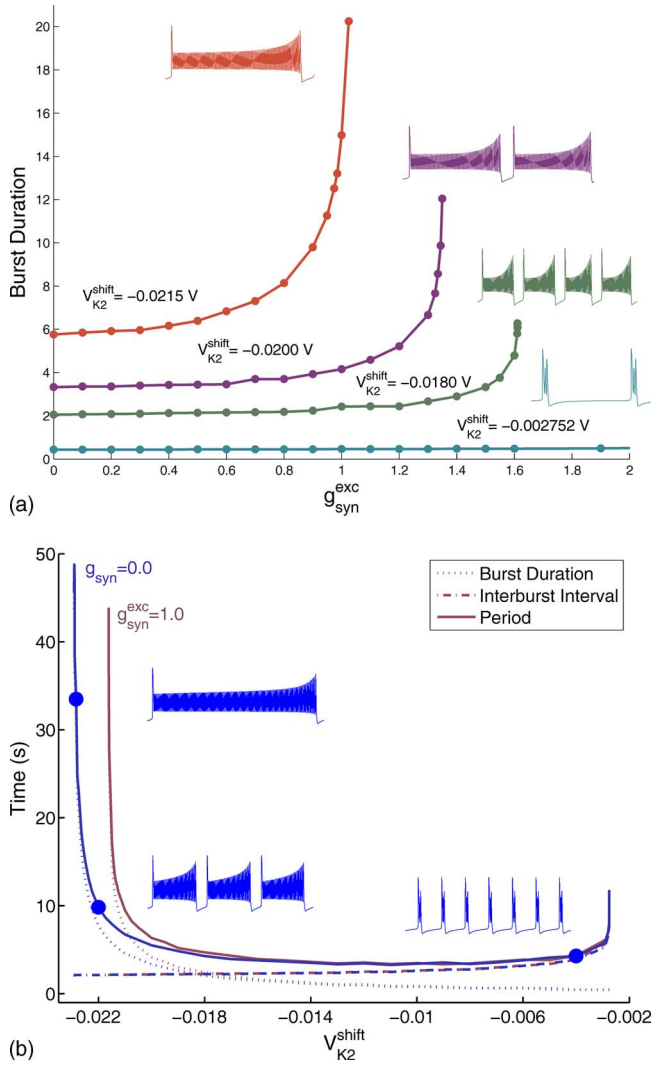

FIG. 3. (Color online) Temporal characteristics of bursting plotted against the control parameters: the intrinsic one V_{K2}^{shift} and the network coupling strength g_{syn}. The burst period increases as either the burst duration or the interburst interval becomes longer through the homoclinic saddle-node or saddle bifurcations near the boundaries SN_{lc} and SN_{eq}, respectively. Both, though, contribute equally only near their intersection point in the bifurcation diagram shown in Fig. 2.

ized state of the interneuron. This stable equilibrium state emerges through the saddle-node bifurcation too, right at the tangency of the slow nullcline $m'=0$ with the quiescence manifold M_{eq} near its hyperpolarized fold.

Both saddle-node bifurcation curves are shown in the bifurcation diagram in Fig. 2. The second bifurcation parameter in this diagram is the effective flux of the incoming synaptic current averaged over its duration $\langle I_{syn}\rangle = 1/\tau_{bd}\left|\int_0^{\tau_{bd}} I_{syn}dt\right|$. This current is treated as an inhibitory or excitatory one, depending on the level of the reversal potential.

In Fig. 2 we single out the zones of activity of the interneurons: bursting, quiescence, and tonic spiking. One sees from this diagram that the interneuron is locked down at the hyperpolarized quiescent state when V_{K2}^{shift} is too large corresponding to the blocked potassium current (m_i close to 0 as Fig. 1 indicates). When the interneuron is locked down, there is a stable equilibrium state on the hyperpolarized branch of the 1D quiescent manifold M_{eq} at its intersection point with the 2D slow nullcline $m'=0$. It is evident that the external inhibitory current facilitates this state as well, while the excitatory one works against it, in contrast, making the interneuron oscillate around the depolarized state. The central part of the bifurcation diagram is occupied by bursting. Right below the boundary SN_{eq} separating the bursting and hyperpolarized quiescence zones, the interburst interval is long, and the burst duration is short, see Fig. 3(b).[12] This is a feature of the saddle-node bifurcation that occurs on SN_{eq} where the space curve M_{eq} and the hypersurface $m'=0$ have a quadratic tangency in the 3D phase space of the model (1). As soon as both are split apart, the dwelling time (read the interburst interval) throughout the phantom of the vanished saddle-node equilibrium state is scaled as $1/\sqrt{\alpha}$, where α is the distance to the bifurcation curve SN_{eq} in the bifurcation plane.

The boundary between bursting and tonic spiking is composite as consists of two branches labeled by BSC and HB_{lc}. The first one is due to the blue-sky catastrophe that describes a homoclinic bifurcation of a saddle-node periodic orbit.[10,48,49] The local component of this bifurcation, taking place on the bifurcation curve SN_{lc}, occurs on the tonic spiking manifold M_{lc}; it leads to the emergence of the two periodic orbits: a saddle one and a stable one. The stable periodic orbit represents the tonic spiking activity of the interneuron. The homoclinic structure of the blue-sky catastrophe is due to recurrent bursting, or more specifically due to the repeated reinjection of the phase point back into the spiking phase after its slow drifting along the hyperpolarized branch of the

quiescent manifold M_{eq}. Likewise the saddle-node bifurcation of the equilibria above, because of the slow passage of the phase point throughout the "phantom" of the saddle-node orbit, the number of spikes within the burst can be arbitrarily large. This makes the burst duration, as well as the period, of the bursting orbit very long as well. The quantitative dependence of the temporal characteristics of the bursting on the parameters is revealed by Fig. 3.

While the blue sky catastrophe on BSC describes a continuous and reversible mechanism of the transition between the bursting and the tonic spiking activities,[10,50] the transition through SN_{lc} and then HB_{lc} gives rise to the onset of the bistability in the model.[11,51,52] Within the wedge bounded by these curves the tonic spiking and the bursting attractors coexist. Their basins of attraction are separated by the stable manifold of the saddle periodic orbit, which has emerged, along with the stable one, to the left from SN_{lc} after the saddle-node bifurcation. The burst period, or more exactly the duration τ_{bd} of bursting becomes longer the closer the bursting orbit approaches this separating saddle periodic orbit, or the closer the parameters are chosen to the boundary HN_{lc}. Correspondingly, the burst duration obeys the scaling law $\tau_{bd} \sim |\log(\alpha)|$, where α is the deviation from the homoclinic bifurcation.

Raising the influx of the excitatory synaptic current seizes the magnitude of the tonic oscillations around the depolarized steady state of the interneuron. This occurs right underneath the boundary AH that corresponds to the Andronov–Hopf bifurcation. Note that between AH and SN_{lc}, the invisible saddle orbit still separates the bursting from a now depolarized steady state attractor.

This orbit sets the threshold as well between the coexistent tonic spiking and the hyperpolarized quiescent activities in the interneuron for the parameter values from the top-left sector of the bifurcation diagram.

The dependence of the temporal characteristics of bursting against the parameters is shown in Fig. 3. It reveals that the growth of the burst period is either due to the increased interburst interval when the interneuron becomes more hyperpolarized, or because of the increase of the burst duration as bursting evolves toward tonic spiking when the interneuron becomes more depolarized (V_{K2}^{shift}), or alternatively, excited by the external current when g_{syn}^{exc} (or $\langle I_{syn}^{exc} \rangle$) is increased.

Of our special interest is bursting of large duty cycles, i.e., when the burst duration is much longer than the interburst interval near the boundary composed of $BSC \cup HB_{lc}$. It follows from the paradigm of the synaptic current modeling that its contribution is more effective when the driving neuron stays active (on) longer above the threshold. In the other, such a bursting neuron is very vulnerable, and hence *highly* sensitive to external perturbations brought in by the synaptic current. In what follows this shall lead to especially peculiar consequences. Namely, whenever the interneuron produces very long bursts, i.e., its parameters correspond to the rapidly increasing segments of the temporal characteristics. A small deviation, either due to the internal parameter V_{K2}^{shift}, or due to an external influence, expressed through effective inward flux $\langle I_{syn} \rangle$, originated from the outer network, shall drastically extend, or shorten the burst period by changing either the burst duration or the interburst interval. We will show below that the interneuron of the longest burst duration becomes a designated pacemaker that determines the pace and the rhythm of the motif, as well as larger CPGs. Moreover the ratio of the burst durations of the composing interneurons becomes the actual order parameter in such networks.

III. INHIBITORY MOTIFS

In this section, we focus on the mechanisms generating antiphase bursting in the simplest network of two reciprocally inhibitory interneurons, and burst synchronization in a three-neuron network with all inhibitory connections. These mechanisms, along with the effect of increasing the neuron's burst duration by excitation, will be used for describing synchronous pattern formation in inhibitory-excitatory networks considered below in Sec. IV.

A. Half center oscillator

Two coupled bursting interneurons with fast reciprocal inhibitory synapsis are known to exhibit an antiphase behavior where interneuron activities alternate in antiphase between a quiescent state and fast repetitive spiking. Such a network with the two interneurons acting in antiphase is called a half-center oscillator[53] (HCO). Such an antiphase behavior is often reported as an integral part of CPG networks governing locomotion patterns, especially if there is antiphase symmetry in the motor outputs.[2]

Next, we will discuss specific properties of the antiphase bursting and the underlying mechanism of its generation in a two-neuron inhibitory network (1) with some relatively small factors g_{12}^{in} and g_{21}^{in}. The mechanism leading to the asynchronous network behavior is similar to that of the formation of a HCO from an oscillating network of two mutually inhibitory interneurons.[22,42]

We consider the type of bursting where the burst duration quite exceeds the interburst interval. Thus, whenever one interneuron is on, the other one gets inhibited and must stay off, provided that the incoming synaptic current is above a certain threshold sufficient to cause the saddle-node bifurcation that gives rise to emergence of the locked down state on the hyperpolarized quiescent branch of the other interneuron (see Fig. 4 and a small HCO pictogram in Fig. 2). By geometry of the nullclines, each uncoupled model (1) always has a unique unstable equilibrium state located away from the stable, hyperpolarized branch of M_{eq}.

A sufficient inhibitory current from the active neuron applied to the postsynaptic neuron shifts M_{eq} towards the slow nullcline $m'=0$ thereby creating, in the phase space of the driven interneuron, a new stable equilibrium around the low, hyperpolarized knee of M_{eq} through a saddle-node bifurcation. We use this stable equilibrium state as the locked down state. We will refer to Fig. 4 to illustrate the mechanism of antiphase synchronization. In this diagram, the inactive interneuron 1 (represented by the blue sphere) remains locked at the low knee of M_{eq} and is hence inactive. Soon after the active interneuron 2 (the green sphere in the figure) falls down below the synaptic threshold after competing the current spiking period of bursting, the inactive one becomes

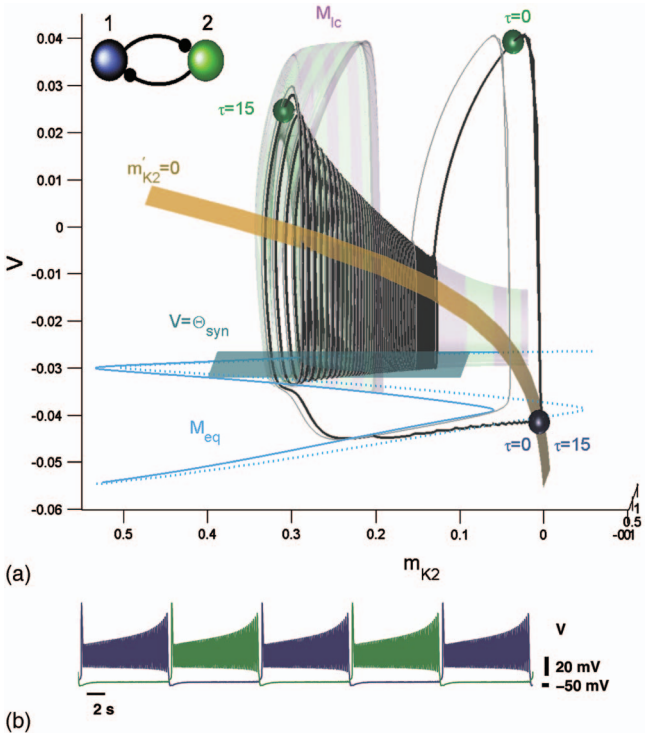

FIG. 4. (Color) Half-center oscillator: the composing interneurons burst in antiphase at $V_{K2}^{shift}=-0.022$, $g_{12}^{in}=0.8$, and $g_{21}^{in}=0.9$. Shown are phase trajectories of the uncoupled interneurons at $g_{syn}=0$ (gray bursting orbit) and the HCO (black bursting orbit). A sufficient synaptic current applied to the driven interneuron translates the quiescent manifold M_{eq} towards the slow nullcline $m'=0$ far enough to make a stable, locked-down state around the right knee of M_{eq} through the tangency of both manifolds at the saddle-node bifurcation. The new, "inhibited" manifold M_{eq} is represented by the blue dotted curve. While the green interneuron is "on," traversing the spiking manifold M_{lc}, it locks down the inactive (blue) interneuron at the new stable equilibrium. After the active green interneuron has eventually reached the end of the spiking manifold and fallen down, the driving inhibition is turned off. This creates the stable equilibrium state, that holds the inactive interneuron at the right knee of M_{eq}, and later disappears through the reverse saddle-node bifurcation. Released from inhibition, the inactive blue interneuron is free to fire action potentials and begins passing slowly throughout the "phantom" of the disappeared saddle-node. Having jumped up off the fold of M_{eq}, it traverses throughout the synaptic threshold Θ_{syn} thereby turning on the inhibition onto the other interneuron of the half-center oscillator. The latter will not escape from inhibition while the blue interneuron is in the active phase. This process of switching between active and inactive states of the two cells becomes cyclic and leads to anti-phase synchrony.

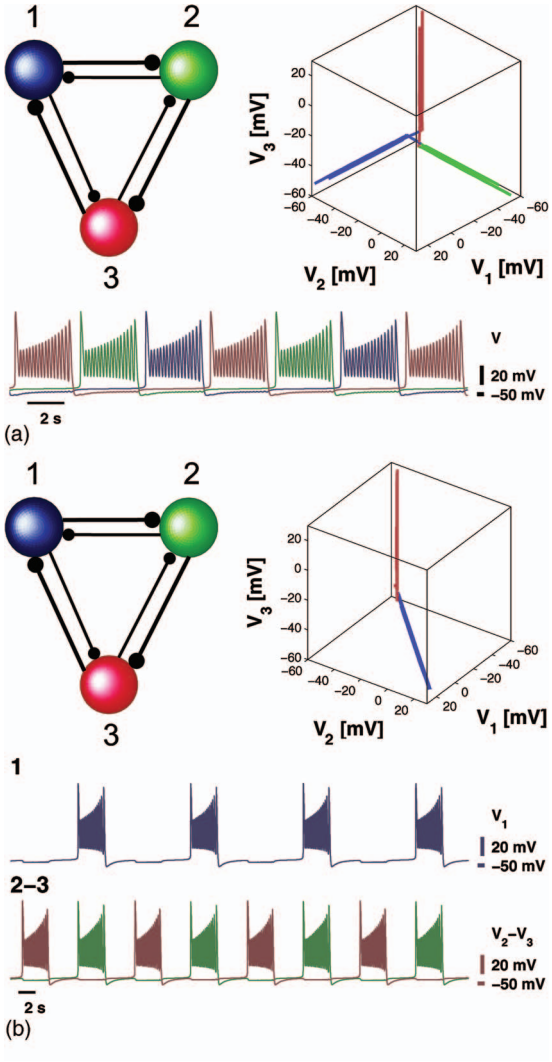

FIG. 5. (Color) Coexistence of cooperative behaviors in the HCO-based inhibitory motif. The coupling parameters are $g_{i,i+1}^{in}=0.9$ and $g_{i+1,i}^{in}=0.62$, and $V_{K2}^{shift}=-0.02$. (a) $2\pi/3$ resonant rhythm where a single interneuron is active at a time. The current configuration of the membrane potential phase space of this motif resembles the $2\pi/3$-resonance, which is not the case as the membrane potential states are truly orthogonal. (b) Burst synchronization between the blue and green interneurons 1 and 2. The 3D membrane potential phase space shows an antiphase between the red and the synchronous HCO composed of the blue and green interneurons. The 3D membrane potential phase space shows an antiphase relationship between the red (3) and the synchronous HCO composed of the blue and green interneurons 1 and 2.

released from inhibitions and begins firing its action potentials. Note that the gap between the nullclines $m'=0$ and M_{eq} in the uncoupled system is small so that a weak inhibitory coupling is even sufficient to close the gap and lock the inactive interneuron at the right knee. For the given network's parameters, the critical value of the inhibitory coupling is $g^*=g_{12}^{in}=g_{21}^{in}=0.017$ such that a coupling exceeding g^* triggers the antiphase synchrony.

The given model of the synaptic current assumes that the connectivity is effectively and temporarily one-directional, meaning that an inactive interneuron has no feedback onto the active one. This implies that for the HCO it is imperative that both interneurons are indeed the bursters. Otherwise, if either interneuron is tonic spiking, the other one becomes permanently locked down, provided that the connectivity strength is sufficient. It is not hard to see from Fig. 2 that this can be easily achieved if the interneuron's parameters happen to be set close to the boundary SN_{eq}. The second peculiar observation is that the interneurons do not have to be identical to form the HCO. If they are, then the burst period of the HCO is double of the burst duration of the interneuron. In an asymmetrical case though, the period of the HCO is the sum of the burst durations of both interneurons, provided that the burst duration of either interneuron exceeds the interburst interval of the other.

B. Unidirectional inhibitory ring

Let us next consider an inhibitory triangle (as one in Fig. 5) with only unidirectional clockwise connections. Note

at once that for this configuration to repetitively produce the cooperative bursting behavior, its interneurons no longer have to be endogenous bursters, but may be spiking ones as well. To illustrate the point, bursters with duty cycle equal to one are chosen. The above *on-off* rule/principle is this case works as follows: let the red interneuron 1 be "on," i.e., fire the series of spikes, then, by the underlying principle, it inhibits the following clockwise blue interneuron that accordingly becomes locked down. On the other hand, for the red interneuron to be active, the preceding green one must temporally be "off" as well, during the given episode. As the result, the inhibitory ring produces the bursting activity qualitatively resembling the $2\pi/3$ resonance where only one interneuron is active at the time.

The firing pattern also persists in the ring with both clockwise and counterclockwise connections (see the section on multistability below). Moreover, it was shown in Ref. 54 that such a bursting alteration can be due to a single attractor composed of heteroclinic connections in the similar inhibitory motif composed of identically spiking neurons described by the original Hodgkin–Huxley equations. In the given context, the absence of multistability is imperative to justify the novel concept of *winnerless* competition resulting in a mono-cooperative behavior of the network without designated pacemakers.[26]

We will shown below that in an even, reciprocally inhibitory motif, this winnerless pace can *coexist* with seven other distinct synchronous patterns, i.e., constitutes one of eight primary attractors of this network.

C. HCO-based motifs

Let us examine the inhibitory triangle with both reciprocal clockwise and counterclockwise connections (Fig. 5). The connections in each direction are not necessary symmetric; moreover let them be stronger in the clockwise direction. Further we will consider an inhibitory triangle with asymmetrical, heterogeneous coupling and discuss the role of asymmetry in establishing distinct cooperative behaviors.

The network shown in Fig. 5 can exhibit up to four coexisting rhythms. In addition to the $2\pi/3$ resonance pace [see Fig. 5(a)] persisting in this bidirectional network too, there exist three other types of polyrhythmic synchronous rhythms where either of the two interneurons are burst synchronized between and antisynchronized with the third interneuron [see Fig. 5(b)]. The manifestation of a particular rhythm depends on the initial states of all three interneurons. The performed simulations of random perturbations of the initial conditions of the interneurons, revealed for the parameter values indicated in the figure, that the $2\pi/3$ resonance rhythm is dominant as its odds are about 82%. The remaining 18% are evenly divided between the configurations, all having a single designated (up to a color coding) pacemaker synchronizing the other two interneurons of the motif.

Next we would like to examine the mechanism leading to the generation of these shift-symmetry synchronous rhythms in detail. In our recent work[28] we discovered a highly counterintuitive result concerning a typical configuration of a bursting motif, which is similar to the one shown in Fig. 5. Specifically, we considered a HCO (code-named "Goliath") composed of two strongly inhibitory interneurons, which are driven weakly by an independent bursting interneuron (code-named "David"). We showed that even a weak inhibition originated from "David" can quickly synchronize the HCO, provided that the burst durations of all three uncoupled interneurons sufficiently exceed the interburst intervals.

In contrast to the "David–Goliath" case, all three interneurons composing the reciprocally inhibitory network shown in Fig. 5 have nearly equal burst durations and interburst intervals, when uncoupled. Hereafter, the parameters of each interneuron of Eq. (1) are chosen to be close to the transition boundary in Fig. 2 separating the bursting and tonic spiking activities, whose upper part is due to the blue sky catastrophe[10] and the low one is due to the bistability scenario.[11] In both cases, the burst duration of the interneuron increases with no bound, as the transition boundary is approached, while the interburst interval stays nearly constant. It is worth noticing again here that near the transition the burst duration is highly sensitive to small variations of the parameters; intrinsic, as well as networking induced by extremal synaptic currents. In the considered case this implies that originally identical interneurons with equal burst durations and interburst intervals may receive unequal inhibitions from each other. It can be seen in Fig. 2 that the incoming inhibition may properly shorten the burst duration of the driven interneuron. More specifically, the burst duration of the interneuron receiving less inhibition shall become longer. Note that despite the fact that each interneuron has the incoming synaptic connections of equal strength, the effective amount of inhibition received by each interneuron may differ, depending on whether the other interneurons are active or not during the current episode of the bursting cycle.

Recall that due to the antiphase behavior of the HCO, either interneuron must stay inactive, being locked down around the hyperpolarized knee of M_{eq}. Consider the HCO composed of neuron 1 (blue interneuron) and 2 (green interneuron) and suppose that neuron 3 (red interneuron) is active; it inhibits the locked down blue interneuron (cf. Fig. 4) of the HCO even further. Meanwhile, the uneven inhibition exchange between the red and green interneurons leads to uneven shortening of the active phases of both active interneurons. When the green interneuron becomes inactive first, the bursting of the red interneuron returns to its natural active pace. Meanwhile, as the latter continues to stay active, its inhibition continues to lock down both HCO (blue and green) interneurons on the hyperpolarized, lower part of the nullcline of M_{eq}. Moreover, the green interneuron moving along the nullcline can and does catch up with the blue interneuron locked at the hyperpolarized knee of M_{eq}. After the membrane potential of the red interneuron lowers below the synaptic threshold, its entering the quiescent phase releases the other two interneurons from inhibition and both begin firing (nearly) simultaneously. While being active, they doubly lock down the red interneuron until the last active interneuron spikes. By doing so, the blue and green interneurons become burst synchronized.

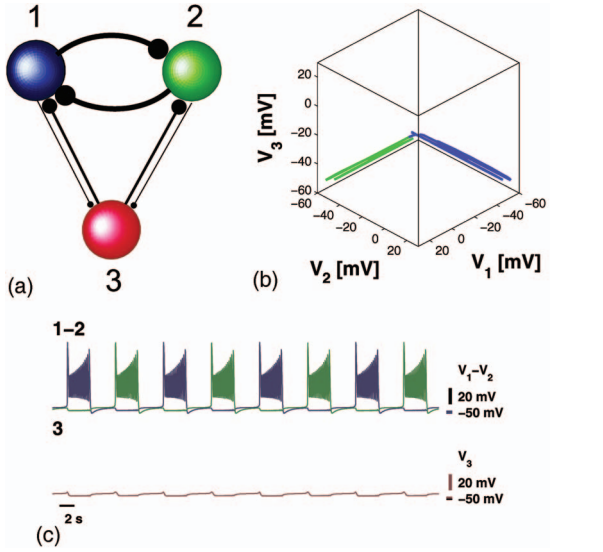

FIG. 6. (Color) Asymmetric inhibitory triangle. The red interneuron is locked down by the HCO composed of the blue and green interneurons, bursting in antiphase. This regime coexists with the synchronous polyrhythmic rhythm, depicted in Fig. 5(b). The coupling parameters are $g_{12}^{\text{in}}=1$, $g_{21}^{\text{in}}=0.8$, $g_{13}^{\text{in}}=0.6$, $g_{31}^{\text{in}}=0.4$, $g_{23}^{\text{in}}=0.5$, and $g_{32}^{\text{in}}=0.3$, and $V_{\text{K2}}^{\text{shift}}=-0.02$ in both cases.

Note that unlike the David–Goliath network,[28] the present all inhibitory network selects its pacemaker by shortening the burst duration of the other "secondary," driven interneurons. However, this polyrhythmic synchronization requires stronger couplings among the interneurons of the motif, and is unreliable because not only does it coexist with two other ones symmetrical up to a shift, but with the dominant $2\pi/3$ resonance rhythm in this clockwise prevailing configuration.

A similar polyrhythmic synchronous rhythm will also occur in an arbitrarily reciprocal motif as one depicted in Fig. 6. The choice of the coupling parameters here is somewhat arbitrary. Due to the asymmetry of the coupling, the single synchronous rhythm can persist here from the symmetrical case. This rhythm has been previously depicted in Fig. 5(b) where the blue and green interneurons composing the HCO are effectively controlled by the red interneuron and thus burst synchronized. In this case there is another type of multistability; this time, it coexists with the regime where the HCO-forming interneurons bursting in antiphase, dominate the dynamics by constantly locking down the red interneuron (see Fig. 6). This becomes possible if the red interneuron was initially inactive so that the alternating on-off states of the green and blue interneurons hold it at the low hyperpolarized knee of M_{eq}. The performed simulations revealed that the odds for the occurrence of these coexisting rhythms are split between 61% for the appearance of the latter rhythm and 39% for polyrhythmic synchronization, respectively. Basically, one may state that the phase space of the network is divided by the attraction basin of the rhythms in proportion about 2/3. Recall that as follows from the way the model (1) is derived, its phase space is bounded naturally; the range for the gating variables (read probabilities) is between 0 and 1, while the realistic range for the membrane voltage is between somewhat 60 and −70 mV.

IV. MULTISTABILITY AND CONTROL OF POLYRHYTHMICITY

In the previous section we have demonstrated various types of polyrhythmicity which the reciprocally inhibitory motifs composed of three bursting interneuron can produce, depending on the strengths of the connections. Each type corresponds to a unique attractor of the motif. Each attractor has its own attraction basin. So depending on the initial condition the phase state of the motif falls into the basin of the selected attractor. The attractors can bifurcate and transform into other more complex ones, where, for example, some driven interneuron can skip the period of bursting, or vice versa, and fire with the double frequency. Such rhythms are out of scope of the given consideration, and need a more systematic, symbolic description. The basin of an attractor also changes together with the changes of the connectivity strengths, and therefore its presence is dictated by networks configurations, so that some attractors may not even exist as, for example, in the case of the unidirectional, inhibitory ring. It is hence clear that the chosen rhythms of the motif depend upon the capacity of the attractor, i.e., its basin. More specifically, to avoid speculations on the "size" of a basin in the 9D phase space of the motif, we can drastically narrow the problem to the phase of the current state of each interneuron on the corresponding bursting orbit. The underlying idea is to make the motif switch from one rhythms to another not by picking randomly initial conditions and following the transients toward some attractor of the network, but to perturb this attractor for a given configuration of the motif by applying an arbitrarily lasting pulse of the (hyper)depolarizing current of adequate magnitude to one of the interneurons.

Due to the periodicity of bursting exhibited by the motif, the ordinal number, or the color of the interneuron can be any; the pulse is applied to the blue interneuron in all three cases. One sees from Fig. 7 and the caption that the motif under consideration is slightly biased against the red interneuron whose feedback onto the other two cells is several times weaker, than the forward inhibition that it receives from them. Nevertheless, this does not prevent it from dominating over the synchronized blue and green interneurons firing simultaneous bursts in antiphase with the driving red one. The external pulse applied to the blue interneuron while it is in "off" state, extends its inactive state, while the red and green ones keep firing in the antiphase manner, becoming the half center oscillator. In what follows, the current phases of the bursting interneurons matter most when the locked down interneuron is released from the external inhibition. In Fig. 7, this occurs when the red interneuron is active and yet delays the inactive phase of the blue interneuron. Shortly thereafter, the red interneuron becomes inactive, the blue one goes "on" and forms the HCO along with the green one. The new established HCO inhibits the formerly dominating red interneuron so that it stays inactive for the rest of the time.

The way the rhythm changes under similar circumstances in a more equally balanced motif is illustrated in Figs. 8 and 9. Here, the original dynamics, which is similar

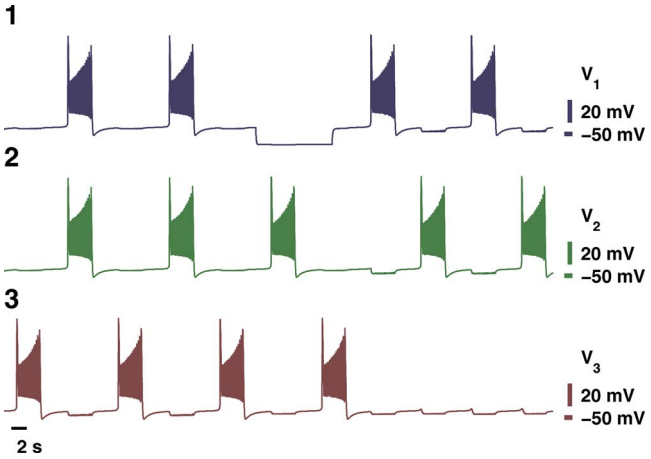

FIG. 7. (Color online) The red interneuron dominating over the synchronous blue and green ones becomes forcefully inactive by the formed HCO after the hyperpolarizing pulse has been applied to the blue interneuron thereby breaking the original rhythm in this asymmetric inhibitory motif with the parameters $g_{12}^{in}=1.1$, $g_{21}^{in}=1.0$, $g_{13}^{in}=0.6$, $g_{31}^{in}=0.1$, $g_{23}^{in}=0.5$, and $g_{32}^{in}=0.1$, and $V_{K2}^{shift}=-0.02$ mV.

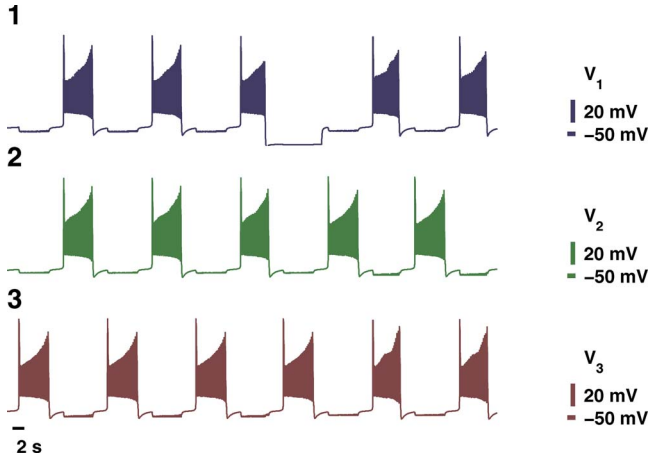

FIG. 9. (Color online) The changing winner in the motif: the red interneuron loses its pacemaker role that goes to the green one after the depolarizing current is over for $g_{12}^{in}=1.0$, $g_{21}^{in}=0.8$, $g_{13}^{in}=0.75$, $g_{31}^{in}=1.1$, $g_{23}^{in}=1.0$, and $g_{32}^{in}=0.77$, and $V_{K2}^{shift}=-0.022$ mV.

to that in the previous example, is featured by the domination of the red interneuron driving the synchronous blue and green ones with even more mismatched connectivity weights. The applied pulse locks down the target interneuron, while the remaining two form the HCO as they keep firing bursts in antiphase. The phase of the interneuron released from inhibition is such that the cooperation of all three interneurons leads to the onset of the so-called winnerless competition dynamics typical to a unidirectional inhibitory ring. Like in the previous example, by releasing the target cell from inhibition at a proper phase, we can have the original dynamics restored in the motif as well.

The last example in this section shows that the winner, or the dominating interneuron, can be designated by applying and releasing the hyperpolarizing pulse off any target cell of the network. After releasing the target cell from inhibition the role of the pacemaker switches to the green interneuron that now leads the other two synchronous interneurons. In a similar manner, we can designate the blue interneuron as a pacemaker by inhibiting and releasing it during proper phase relative to the current phases of the rest. We should observe that, in contrast to the first two examples, the connectivity weights in this case are distinct; so that does give priority to the winner, not to winnerless dynamics, as there is no certain asymmetry required to have the above type of dynamics established in the motif.

It is not hard to see that such a regular motif can potentially exhibit up to eight primary rhythms including three winner cases, three "loser" cases with a single interneuron permanently down, as well as to the winnerless competition dynamics where a single interneuron is active at a time. The eighth rhythm is totally symmetric and occurs therefore in an almost equally weighted motif where all three interneuron fire in synchrony. There are some other peculiar though less commonly occurring rhythms that the motif can produce. We plan to analyze those in detail in the next paper.

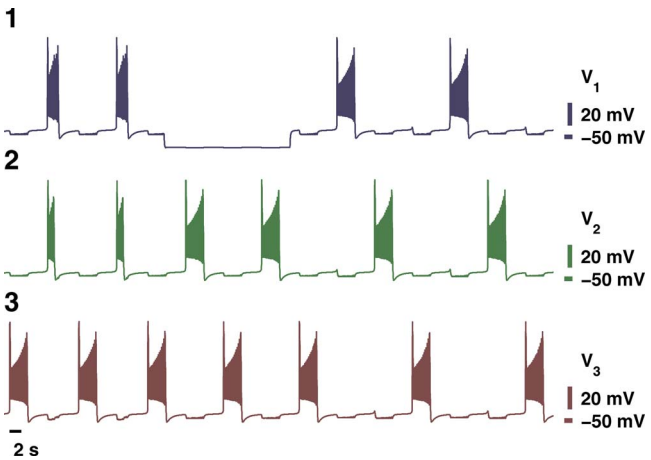

FIG. 8. (Color online) From winner to winnerless dynamics in the motif with asymmetrically weighted connection: $g_{12}^{in}=1$, $g_{21}^{in}=0.75$, $g_{13}^{in}=0.75$, $g_{31}^{in}=1.0$, $g_{23}^{in}=1$, and $g_{32}^{in}=0.75$, and $V_{K2}^{shift}=-0.02$ mV. The driving interneuron loses its superiority after the application of the external hyperpolarizing pulse to the driven interneuron. The original status can be restored as well.

V. INHIBITORY-EXCITATORY MOTIFS

As discussed above, purely inhibitory motifs of neurons (1) with equal burst durations and interburst intervals can self-organize synergistically and designate a synchronizing pacemaker. However, the induced synchronous rhythms typically coexist with asynchronous ones. In this section, we show that the addition of excitatory connections is required to ensure robust synchronous rhythms.

A. Inhibitory-excitatory pair

The inhibitory-excitatory configuration shown in Fig. 10 has the following two important properties. First, it can burst-synchronize the interneurons, i.e., the start of their tonic spiking phases. Second, it may shorten (increase) drastically the burst duration of the inhibited (excited) interneuron, provided that the control parameter V_{K2}^{shift} is set close to the bifurcation value corresponding to the transition from bursting into tonic spiking activity.

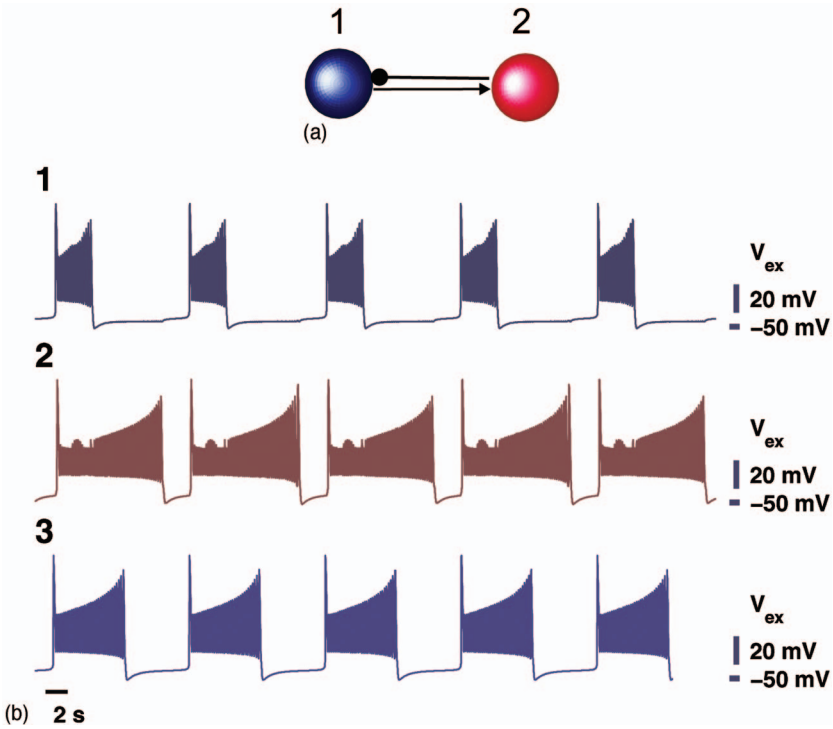

FIG. 10. (Color) Inhibitory-excitatory pair and the voltage traces at $V_{K2}^{shift}=-0.022$, $g_{21}^{in}=0.4$, $g_{12}^{exc}=0.2$: The bottom, reference trace 3 shows the natural frequency of uncoupled bursting, compared to it, the burst duration of the red interneuron grows due the excitation it gains from the blue interneuron, whose burst duration is in turn shortened by the reverse inhibition. When the blue interneuron becomes active, it turns the red interneuron on as well. In turn, the red interneuron shortens the burst duration of the blue interneuron. After the blue interneuron becomes inactive, the red interneuron restores the natural rate and continues as an uncoupled interneuron. This sharp change can be seen in its voltage traces aligned with the bursting termination of the excitatory blue interneuron.

The onset of the burst synchronization in this network can be explained as follows. Let the inhibiting, red interneuron be active at the moment, i.e., the corresponding red phase point drifts turning around the spiking manifold M_{lc} and hence locks down the blue interneuron near the hyperpolarized fold on the quiescent manifold M_{eq}. The development is initially identical to that in Fig. 4. Observe that when the blue interneuron is inactive, the excitatory synaptic coupling is turned off so it sends no feedback to the active red interneuron for a moment. After the red interneuron reaches the end of M_{lc} and falls down to M_{eq}, and its inhibition toward the blue interneuron is turned off. As in the case of the HCO network, the blue interneuron, released from inhibition, is ready to jump up after a slow passage throughout the phantom of the vanished, inhibition-induced equilibrium state. Meanwhile, the red interneuron traverses along the unperturbed M_{eq} toward its hyperpolarized fold. When the blue interneuron eventually takes off M_{eq} becoming active, then it switches excitation onto the red interneuron. Moreover, in contrast to the inhibitory case, this moves the fold of the perturbed quiescent manifold M_{eq} toward the current position of the red interneuron thereby *shortening* its quiescent period (state). This leads to that the red interneuron is forced to follow the blue, exciting interneuron right after the latter becomes active so that both interneurons begin firing action potentials nearly synchronously, with a short delay of order of two spikes or so, provided the excitatory coupling is sufficient: $(g^e > g^* = 0.06)$. However, while the interneurons are active, they follow different routes. The red interneuron, while excited, has a longer burst duration and has a longer distance to go along the perturbed tonic spiking manifold; see Fig. 1. At the same time, the route of the interneuron receiving the inhibition originated from the red one becomes shorter in contrast. Furthermore, after it becomes inactive, its feedback faints, and the red interneuron continues firing with the natural frequency. This explain the disturbances in the beginning of each burst in its voltage trace in Fig. 10 which occur while the excitatory interneuron is still "on." Therefore, despite the interneurons which fall down from the spiking manifold M_{lc} at different times and position in the phase space, they nevertheless become burst-synchronized again after the excitatory blue interneuron begins the new cycle of bursting. This burst synchronization between the excitatory and inhibitory interneurons is demonstrated in Fig. 10.

B. Inhibitory-excitatory HCO-based motifs

The emergence of the synchronous rhythm in the mixed network depicted in Fig. 11 is determined by the same synergetic mechanisms described in the previous sections. These are the "lock-down-then-release" mechanism of inhibition, then the induced burst synchronization as in the inhibitory-excitatory pair, and the extension of the burst duration in the excited (inhibitory) interneuron.

The development and onset of the burst synchronization among all three interneurons, supplemented by complete synchronization between the strongly inhibitory ones forming the HCO, is shown in Fig. 11. To explain its emergence, we suppose, without loss of generality, that the red interneuron receiving the excitation from the HCO is initially active, i.e., on the tonic spiking manifold M_{lc} (cf. Fig. 4). In addition let the blue interneuron be active, too. Clearly if the green interneuron were inactive, it should remain such, locked down near the fold on the quiescent manifold M_{eq} by the inhibition generated by both active interneurons. Furthermore, due to the excitation generated from the blue interneuron, the red one stays active longer, and hence its burst duration becomes longer than that of the blue one. On the

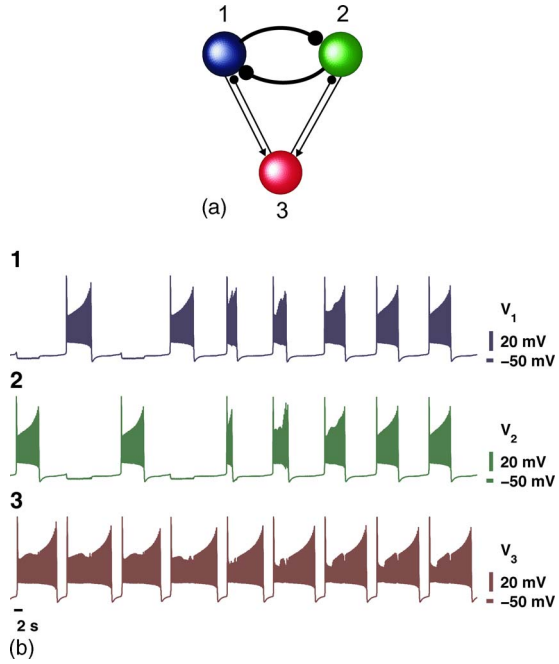

FIG. 11. (Color online) Three-interneuron network with both inhibitory and excitatory synapses. Solid circles indicate the direction of inhibitory coupling; arrows show the direction of excitatory coupling. Excitatory synapses increase the burst duration of neuron 3, making it the pacemaker synchronizing the HCO formed by neuron 1 and 2. Corresponding voltage traces show the onset of the polyrhythmic synchronous rhythm. Parameters are $g_{12}^{\text{in}}=1=g_{21}^{\text{in}}=1$, $g_{13}^{\text{exc}}=0.15$, $g_{23}^{\text{exc}}=0.1$, $g_{31}^{\text{in}}=0.1$, $g_{32}^{\text{in}}=0.1$, and $V_{\text{K2}}^{\text{shift}}=-0.02$ mV. One see that once the antiphasic HCO is forced by the red pacemaker, it becomes fully synchronous. Observe, that the strong reciprocal inhibition within the HCO makes its burst duration much shorter and extends that of the pacemaker receiving now double excitation from the in-phase interneurons.

contrary, its generated inhibition shortens the active phase of the blue interneuron in a similar manner (refer to Fig. 1), that reaches the edge of the spiking manifold way ahead of the red one, to become inactive. While inactive, it traverses the hyperpolarized manifold M_{eq} toward its fold to catch up with the green interneuron which remains locked.

The next phase in the development of the synchronous rhythm is similar that of the inhibitory-excitatory pair discussed above. Thus, after the red interneuron becomes inactive and releases the blue and green interneurons off the

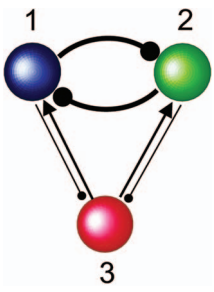

FIG. 12. (Color) Puzzle: What polyrhythmic pattern occurs in the given network? The width of the links may be thought of as the coupling strength. The choice of the coupling parameters is only constrained to the threshold values of the inhibitory and excitatory couplings, required to "lock-down-then-release" and speed up and increase the burst duration of the interneurons, respectively.

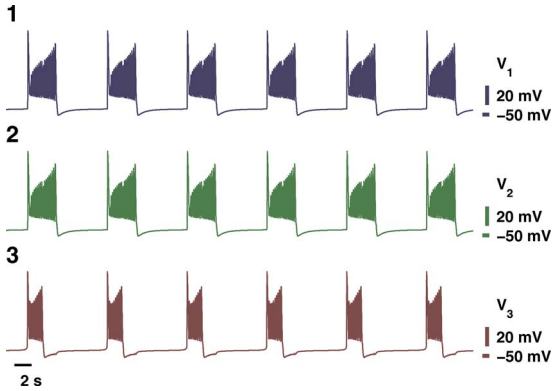

FIG. 13. (Color online) Answer to the puzzle: Burst synchronization among all interneurons. The excitation originated from the red interneuron breaks down the antiphase rhythm of the HCO and triggers burst synchrony through a similar mechanism described for the inhibitory-excitatory pair. Here, $g_{12}^{\text{in}}=0.9$, $g_{21}^{\text{in}}=0.92$, $g_{13}^{\text{in}}=0.52$, $g_{23}^{\text{in}}=0.5$, $g_{31}^{\text{exc}}=g_{32}^{\text{exc}}=1$.

locked down state, both jump up, turning the excitation on toward the red interneuron and forcing it leave the quiescent state and becomes active as well. A sufficiently strong excitation makes this induced synchronous rhythm robust and achievable from nearly all initial states of all interneurons involved in this motif.

We conclude this subsection by the puzzle on the dynamics of the motif shown in Fig. 12. In this figure, the directions of inhibitory and excitatory connections between the HCO and the red interneuron are now reversed. The cooperative dynamics of this network are, as above, determined by the same universal principles. We invite the reader to figure the eventual rhythm matching this network (see Fig. 13 for the answer).

C. Seven-interneuron network

We use the asymmetric network depicted in Fig. 14 as an example that shows the ultimate role of a single excitatory connection from the pacemaker in synchronizing the other interneurons of the network.

Consider first the case where the excitatory connection from interneuron 1 to interneuron 7 is missing, i.e., the whole network is entirely an inhibitory one. Due to the given connectivity diagram, interneuron 7 is a common inhibitor of

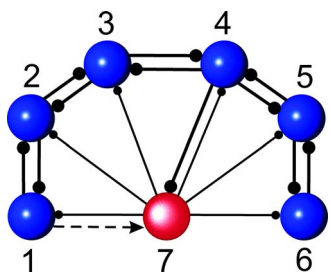

FIG. 14. (Color online) Asymmetric 6+1 interneuron network. In the absence of the excitatory connection (dashed line), the network exhibits asynchronous behavior. The addition of the excitatory designates neuron 7 as the pacemaker leading the burst synchronization of the entire network because of the feedback from its blue subnet; here the coupling weights are $g_{12}^{\text{in}}=g_{21}^{\text{in}}=g_{23}^{\text{in}}=g_{32}^{\text{in}}=1$, $g_{34}^{\text{in}}=g_{43}^{\text{in}}=g_{45}^{\text{in}}=g_{54}^{\text{in}}=g_{56}^{\text{in}}=g_{65}^{\text{in}}=1$, $g_{7j}^{\text{in}}=0.2$, $j=\overline{2,6}$, $g_{47}^{\text{in}}=0.6$, $g_{17}^{\text{exc}}=0.4$, and $V_{\text{K2}}^{\text{shift}}=-0.022$.

the other interneurons and can potentially play the role of a pacemaker, inducing a single synchronous rhythm within the network. This may not be the case if its burst duration is long but not sufficient enough to lock down, accordingly, all other interneurons near the hyperpolarized knee of the quiescent manifold M_{eq} and, hence, to establish any burst synchronization within the subnetwork, composed of the driven blue interneurons (see Fig. 14).

In contrast, the addition of a single excitatory connection (depicted by the dashed directed line) toward interneuron 7, can dramatically change the network behavior due to the following synergetic effect. First, provided that the bursting interneuron 7 is already close to the transition into tonic spiking, the influx of excitation essentially enhances its burst duration, thus making it the pacemaker inducing the burst synchronization within the driven subnetwork. Second, this excitation does synchronize the pacemaker with the subnetwork as well, through the mechanism discussed in Sec. IV. Thus, the network behavior changes synergistically from some uncorrelated asynchronous rhythms to the burst synchronization of the entire network. The voltage traces showing burst synchronization within the subnetwork should be qualitatively similar to those shown in Fig. 11.

Note finally that inhibition which the red pacemaker receives from interneuron 4 can be effectively stronger than the excitation it received from interneuron 1 ($g_{47}^{in}=0.6$ versus $g_{17}^{exc}=0.4$). Nevertheless, as follows from the bifurcation diagram in Fig. 2, the interneuron is more sensitive to the excitatory input extending further its burst phase compared to its shortening if the same interneuron receives an effectively equal influx of the inhibitory current instead.

VI. CONCLUSIONS AND FURTHER DIRECTIONS

We have considered a class of the mixed inhibitory-excitatory motifs, which are the building blocks for larger-sized central pattern generators controlling the locomotion of animals. The comprehensive understanding of pattern formation in neural motifs is gained through the prism of the bifurcation theory giving insights for transformation and transitions between various types of activity of individual and coupled interneurons.

Among all types of bursting neurons, we have focused our consideration on interneurons belonging to the class of the so-called square-wave bursters. Elliptic bursters reported, for example, in the basal ganglia as GPe and GPi cells, remained off the scope of our consideration. We plan to examine motifs composed of such cells in our next research.

We found that the bursting cells with the longest burst durations are the natural pacemakers for inhibitory-excitatory small networks. The ratio of the burst durations is actually the order parameter that quantifies the dynamics of the network and identifies its pacemaker. It carries the composite meaning incorporating both intrinsic properties of individual cells, as well as networking parameters of coupled cells in the network. We employ the burst-interburst interval ratio to control the onset of different synchronous patterns in inhibitory networks. We have created the comprehensive description of polyrhythmic synchronization in inhibitory-excitatory motifs of bursting neurons. We have also discussed the complimentary roles of inhibitory and excitatory connections in synchronizing the network, composed of the interneurons whose states are close to the transition from bursting into tonic spiking. We have demonstrated that the composition of the burst-duration-based mechanisms enables flexible synchronous properties of small neuronal networks.

We have described the universal mechanisms of synergetic formations of synchronous patterns observed in inhibitory-excitatory networks and shown that temporal characteristics of bursting interneurons and the means of their control are a crucial procedure for synchronization of bursting interneurons. In particular, we have shown that a network of bursting neurons initially having the same burst duration and having no designated pacemakers can self-organize and determine the emergent synchronous behavior, by creating its pacemaker with a longer burst duration. The emergent pacemaker, being the longest bursting interneuron, typically receives the maximum amount of excitation, or the minimal influx of inhibition, and determines the network's paces and rhythms.

It was demonstrated that the dynamics of networks composed of monobursting cells is very rich and, furthermore, is not mono, but multistable in essence. So, a simple motif with nearly identical reciprocally inhibitory connections can exhibit a total of eight attractors corresponding to eight distinct types of the polyrhythmic synchronization. Every attractor of the network corresponds to a specific rhythm and is conjectured to be associated with a particular type of CPG locomotive activity. For the details, we refer the reader to a comprehensive review in Ref. 55.

ACKNOWLEDGMENTS

This work was supported by the GSU Brains and Behavior program and RFFI Contract No. 050100558.

[1] L. Glass, Proc. Natl. Acad. Sci. U.S.A. **102**, 10409 (2005).
[2] E. Marder and R. L. Calabrese, Physiol. Rev. **76**, 687 (1996).
[3] C. M. Gray and W. Singer, Proc. Natl. Acad. Sci. U.S.A. **86**, 1698 (1989).
[4] M. Bazhenov, M. Stopfer, M. Rabinovich, R. Huerta, H. D. I. Abarbanel, T. J. Sejnowski, and G. Laurent, Neuron **30**, 553 (2001).
[5] M. R. Mehta, A. K. Lee, and M. A. Wilson, Nature (London) **417**, 741 (2002).
[6] J. Rinzel, *Lecture Notes in Biomathematics* (Springer-Verlag, Berlin, 1987), Vol. 71, pp. 251–291.
[7] D. Terman, SIAM J. Appl. Math. **51**, 1418 (1991).
[8] V. N. Belykh, I. V. Belykh, M. Colding-Joergensen, and E. Mosekilde, Eur. Phys. J. E **3**, 205 (2000).
[9] E. M. Izhikevich, Int. J. Bifurcation Chaos Appl. Sci. Eng. **10**, 1171 (2000).
[10] A. Shilnikov and G. Cymbalyuk, Phys. Rev. Lett. **94**, 048101 (2005).
[11] A. Shilnikov, R. Calabrese, and G. Cymbalyuk, Phys. Rev. E **71**, 056214 (2005).
[12] P. Chanell, G. Cymbalyuk, and A. Shilnikov, Phys. Rev. Lett. **98**, 134101 (2007).
[13] E. M. Izhikevich, SIAM Rev. **43**, 315 (2001).
[14] C. van Vreeswijk and D. Hansel, Neural Comput. **13**, 959 (2001).
[15] M. Dhamala, V. K. Jirsa, and M. Ding, Phys. Rev. Lett. **92**, 028101 (2004).
[16] I. Belykh, E. de Lange, and M. Hasler, Phys. Rev. Lett. **94**, 188101 (2005).
[17] X.-J. Wang and J. Rinzel, Neural Comput. **4**, 84 (1992).
[18] D. Golomb and J. Rinzel, Phys. Rev. E **48**, 4810 (1993).
[19] D. Terman, N. Kopell, and A. Bose, Physica D **117**, 241 (1998).
[20] R. C. Elson, A. I. Selverston, H. D. I. Abarbanel, and M. I. Rabinovich, J. Neurophysiol. **88** 1166 (2002).

[21]J. Rubin and D. Terman, SIAM J. Appl. Dyn. Syst. **1**, 146 (2002).
[22]N. Kopell and G. B. Ermentrout, in *Handbook of Dynamical Systems*, edited by B. Fiedler (Elsevier, Amsterdam, 2002), Vol. 2, pp. 3–54.
[23]T. Lewis and J. Rinzel, J. Comput. Neurosci. **14**, 283 (2003).
[24]N. Kopell and G. B. Ermentrout, Proc. Natl. Acad. Sci. U.S.A. **101**, 15482 (2004).
[25]M. Bazhenov, N. Rulkov, J.-M. Fellous, and I. Timofeev, Phys. Rev. E **72**, 041903 (2005).
[26]M. I. Rabinovich, P. Varona, A. I. Selverston, and H. D. I. Abarbanel, Rev. Mod. Phys. **78**, 1213 (2006).
[27]J. Rubin and D. Terman, Neural Comput. **12**, 597 (2000).
[28]I. Belykh and A. Shilnikov, "When inhibition synchronizes strongly desynchronizing networks of bursting neurons," Phys. Rev. Lett. (accepted).
[29]G. S. Cymbalyuk, Q. Gaudry, M. A. Masino, and R. L. Calabrese, J. Neurosci. **22**, 10580 (2002).
[30]O. Spoorns and R. Kötter, PLoS Biol. **2**, e369 (2004).
[31]R. Milo, S. Shen-Orr, S. Itzkovitz, N. Kashtan, D. Chklovskii, and U. Alon, Science **298**, 824 (2002).
[32]M. Barahona and L. M. Pecora, Phys. Rev. Lett. **89**, 054101 (2002).
[33]V. N. Belykh, I. V. Belykh, and M. Hasler, Physica D **195**, 159 (2004).
[34]I. V. Belykh, V. N. Belykh, and M. Hasler, Physica D **195**, 188 (2004).
[35]L. Zemanova, C. Zhou, and J. Kurths, Physica D **224**, 202 (2006).
[36]I. Lodato, S. Boccaletti, and V. Latora, Europhys. Lett. **78** 28001 (2007).
[37]A. Yu. Pogromsky, G. Santoboni, and H. Nijmeijer, Physica D **172**, 65 (2002).
[38]I. V. Belykh, V. N. Belykh, K. V. Nevidin, and M. Hasler, Chaos **13**, 165 (2003).
[39]M. Golubitsky, I. Stewart, and A. Torok, SIAM J. Appl. Dyn. Syst. **4**, 78 (2005).
[40]M. Golubitsky and I. Stewart, Bull., New Ser., Am. Math. Soc. **43**, 305 (2006).
[41]Y. Wang and M. Golubitsky, Nonlinearity **18**, 631 (2005).
[42]V. Matveev, A. Bose, and F. Nadim, J. Comput. Neurosci. **23**, 169 (2007).
[43]G. S. Cymbalyuk and R. L. Calabrese, Neurocomputing **38–40**, 159 (2001).
[44]D. Somers and N. Kopell, Biol. Cybern. **68**, 393 (1993).
[45]A. N. Tikhonov, Mat. Sb. **22**, 193 (1948).
[46]L. S. Pontryagin and L. V. Rodygin, Sov. Math. Dokl. **1**, 611 (1960).
[47]N. Fenichel, J. Differ. Equations **31**, 53 (1979).
[48]D. V. Turaev and L. P. Shilnikov, Dokl. Math. **51**, 404 (1995).
[49]A. Shilnikov, L. Shilnikov, and D. Turaev, Mosc. Math. J. **5**, 205 (2005).
[50]A. Shilnikov and G. Cymbaluyk, Regular Chaotic Dyn. **3**(9), 281 (2004).
[51]A. L. Shilnikov, R. Calabrese, and G. Cymbaluyk, Neurocomputing **65**, 869 (2005).
[52]G. Cymbalyuk and A. L. Shilnikov, J. Comput. Neurosci. **18**, 255 (2005).
[53]T. G. Brown, Proc. R. Soc., London, Ser. B **84**, 308 (1911).
[54]T. Nowotny and M. I. Rabinovich, Phys. Rev. Lett. **98**, 128106 (2007).
[55]K. L. Briggman and W. B. Kristan, Jr., Annu. Rev. Neurosci. **31**, 271 (2008).